Full-field Representation of Discretely Sampled Surface Deformation for Displacement and Strain Analysis

by M.A. Sutton, J.L. Turner, H.A. Bruck and T.A. Chae

ABSTRACT—A detailed evaluation of the feasibility of determining displacements and displacement gradients from measured surface displacement fields is presented. An improved methodology for both the estimation and elimination of noise is proposed. The methodology is used to analyze the gradients for three tests: (1) uniform rotation, (2) uniform strain, and (3) crack-tip displacement fields. Results of the study indicate that the proposed methodology can be used to extract the underlying two-dimensional displacements and their corresponding gradients from the noisy data with reasonable accuracy. Specifically, it is shown that (a) the digital correlation method for acquiring displacement fields has an error in strain of approximately 150 μstrain at each point, (b) the average strain in a region of uniform strain has much less error, typically on the order of 20 μstrain, (c) the displacement 'noise' present in digital correlation is very small, approximately 0.01 pixels, (d) the proposed methodology for reducing noise in the data is essential to the accurate evaluation of displacement gradients and (e) the successful evaluation of displacement and displacement gradients for all three cases indicates that the proposed methodology can be used both to quantify the displacement fields and to reasonably estimate the overall gradient trends.

Introduction

Experimental data are often obtained to identify and characterize phenomena in scientific and engineering research. Very often, the equipment or technique used to obtain the data have inherent limitations which manifest themselves as noise in the data. The researcher then becomes concerned with interpreting the noisy data. When the noise level is significantly smaller than the value of the noiseless data, the data can be visually smoothed and interpretation of the data is generally not a major problem. However, when the noise is at such a level that the noisy data become too ambiguous to interpret, then some technique is required to identify, characterize, and remove the noise from the data without altering the character of the underlying signal.

Least-squares algorithms have been shown to be effective noise eliminators. Their biggest drawback has been that they require some initial knowledge of the functional form that the smoothed data will assume. Fourier filtering has been used to characterize and eliminate noise. However, the smoothed signals are often not as accurate as one desires. Segalman *et al.*[1] developed an alternative smoothing technique using least-squares and spline functions with finite-element analysis to smooth two-dimensional displacement data acquired in a single direction with moire interferometry. By varying a smoothing parameter, ϵ, this technique controls the degree of smoothing done by the spline functions. More recently, Feng and Rowlands[2] have proposed a finite-element based smoothing algorithm that can smooth one, two or three displacement components. The method uses a functional that involves the sum of square of the second partial derivatives to implement smoothing. Rowlands, Winters and Jensen[3] have used B-splines and a regression approach to smooth data. Tessler *et al.*[4] developed a finite-element method to smooth data that uses the penalty function to enforce a 'continuity' in slopes throughout the field, while using a C° assumption for the underlying elements.

In each case, a method for estimating the choice of smoothing parameter to obtain an optimal smoothing parameter is needed. Segalman[1] suggested a method for choosing the smoothing parameter, but no mathematical basis for the method of choice was given. Chambless *et al.*[5] used a variation of Segalman's technique on displacement data acquired using holographic interferometry.

Even though many different methods can be used to smooth data, the choice of smoothing parameter is left to the investigator's discretion. The subjective choice of a smoothing parameter can lead to inaccurate reconstruction of the noiseless data. A smoothing technique that quantitatively chooses an unbiased, optimum smoothing parameter by utilizing the character of the noise to be eliminated is preferred.

Wahba[6,7] has developed a smoothing method which also uses spline functions and least squares to smooth noisy data. More importantly, Wahba has determined that an optimum smoothing parameter exists for data with random noise which can be determined by minimizing the residual difference between the data without noise and the smoothed noisy data. When the data without noise and/or the actual noise level are not known, then she has proposed that generalized cross validation (GCV) be used to determine the optimum smoothing parameter. Busby and Dohrmann[8] have written an efficient smoothing program that uses GCV to optimally smooth one-dimensional noisy data. A recent extension of the one-dimensional GCV algorithm to two dimensions by Busby and Dohrmann[9] was implemented by using two, sequential one-dimensional smoothings of the data. The method has many advantages. It works well with large data sets. It determines an optimal smoothing parameter internally. It also provides cubic spline fits to the data. Discussions with Dr. Busby have indicated that, as with the one-

M.A. Sutton (SEM Member) is Associate Professor, University of South Carolina, Department of Mechanical Engineering, Columbia, SC 29208. J.L. Turner (SEM Member) is Senior Research Engineer, Firestone, Central Research Lab., 1100 Firestone Parkway, Akron, OH 44317. H.A. Bruck is Graduate Student, California Tech., Mail Code 105-50, Pasadena, CA 91125. T.L. Chae is Graduate Intern, Savannah River Site, Building 773A A0249, Aiken, SC 29803.

Original manuscript submitted: July 12, 1989. Final manuscript received: March 28, 1991.

dimensional GCV program, the method requires a large amount of data when the noise is small. Also, a slight disadvantage to the program is that the data region must be rectangular; this does present problems near curved surfaces.

A smoothing methodology is proposed here to optimally smooth noisy two-dimensional displacement data. This technique requires a two-step analysis of the data. First, a one-dimensional GCV program (the Busby-Dohrmann algorithm) is used to estimate the noise level in the data by sampling multiple rows and columns in the data field. Next, to provide both the capability of handling curved boundaries and also to impose the equations of equilibrium as a constraint, a computer program based on the penalty finite-element method for planar elastic problems is used to smooth the data in two dimensions until the noise level between the final fit and the raw data matches the noise estimate obtained using the GCV analysis. The proposed methodology was evaluated using three separate tests: (1) uniform rotation, (2) uniform strain, and (3) a crack-tip displacement field. In all three cases, experimental data are acquired using the technique of digital image correlation.[10-11] In addition, for case (3) a theoretical solution for a plane strain, K_I displacement field, with computer-generated Gaussian noise superimposed, was analyzed. Results from smoothing of these data provide a controlled evaluation of the smoothing technique's ability to handle noisy, experimental crack-tip displacement data. It is shown that the smoothing technique (a) provides substantial improvement in the quantitative smoothness of the displacement fields and (b) is absolutely essential to obtain reasonable estimates of the trends in the gradients.

The Proposed Smoothing Technique

A complete description of Wahba's smoothing technique using the GCV method is given in Refs. 6 and 7. The GCV method can be used to provide an optimized, smooth fit to a sample of one-dimensional data extracted from the two-dimensional data field. The proposed methodology for determining noise levels in a data set and then reducing the noise is as follows.

(1) Lines of u and v displacement are extracted from the x and y directions. Typically 40 lines in each direction are used for the u and v displacements, with approximately 30 points per line. If more data can be obtained, then the smoothing process should be more effective.

(2) Each line of data is analyzed by the one-dimensional GCV program to obtain an optimal fit. Using the optimal fit, the standard deviation for each line is computed.

(3) The average of the standard deviations for all u and v line sets, designate σ_d, is used as the optimum level of infidelity for the two-dimensional smoothed fit.

(4) The raw u and v displacement data are analyzed by a two-dimensional, penalty-method finite-element algorithm. The smoothing parameter is varied until the standard deviation between the data and the smoothed fit is equal to σ_d.

(5) The smoothed data field is then used as the 'best' estimate of the 'noiseless' two-dimensional displacement data. The fitted displacement field is differentiated to provide the estimated 'noiseless' displacement gradients.

Penalty-method Finite-element Algorithm

Step (4) in the smoothing methodology requires a two-dimensional smoothing algorithm for the u,v displacement fields. Though any of the methods outlined in Refs. 1-4 can be used, a computer program was developed for data smoothing based on a finite-element plane-elasticity analysis and a penalty method.[5] The concept involves minimization of a modified potential energy function of the form

$$\Psi = P + V \tag{1}$$

where

$P = \frac{1}{2}\sum_{i=1}^{n} R_i[d_i - \overline{d_i}]^2$, the penalty function
V = potential energy function for the plane-elasticity finite-element model
$\overline{d_i}$ = displacement, strain or stress components to be imposed at points i (experimentally measured u or v displacements in this application)
d_i = smoothed solution value for $\overline{d_i}$
n = number of points, i, at which constraint (experimental) data are specified
R_i = penalty (weighting) parameter specified for each point i

Minimization of the penalty function P represents a standard weighted least-squares criterion for smoothing the data. It is emphasized that V is defined to be the actual strain-energy function for a finite-element model of an elastic medium. Hence, minimization of Ψ attempts to satisfy two-dimensional equilibrium by also minimizing V. It is this fact that distinguishes the smoothing algorithm developed for this work from those given in Refs. 1, 3, 4 and 9. Thus, in the absence of P, the solution obtained by minimizing eq (2) represents the elastic, finite-element solution for the region of interest, consistent with the applied boundary conditions.

It is noted that the penalty function can be modified to include constraints other than displacements (such as stress or strain boundary conditions) that would provide improved elasticity solutions when solving for the minimum in eq (1). Reference 13 demonstrates an example of this capability.

The R_i values determine the extent to which the constraints are imposed. For $R_i = 0$, the constraints are ignored and a pure elastic equilibrium solution is obtained. For sufficiently large R_i, the constraints are met to the greatest degree possible. Thus the R_i values can be regarded as smoothing parameters. The method permits variable weighting values for each point. However, it is common to use a single penalty parameter for all constraint points, unless there is justification for differential weighting of the experimental data.

The numerical, finite-element implementation of the algorithm is similar to that reported in Refs. 2, 14 and 15. The d_i values are expressed in terms of element nodal degrees of freedom as

$$d_i = [C(x_i, y_i)]\,\{D\}_e \tag{2}$$

where $[C]$ is a row of shape functions evaluated at point i in element e and $\{D\}_e$ is a column of element degrees of freedom. Using eq (2), the modified potential function for a single element takes the form

$$\psi_e = V_e + \tfrac{1}{2}\{D\}_e^T[K^*]_e\{D\}_e - \{D\}_e^T\{f^*\}_e + \left(\frac{1}{2}\right)\sum_{i=1}^{n} R_i\overline{d_i}^2 \tag{3}$$

where

$$[K^*]_e = \Sigma R_i [C]^T [C]$$

$$\{f^*\}_e = \sum_{i=1}^{n} R_i [C]^T \overline{d_i}$$

and the element elastic potential energy is

$$V_e = \tfrac{1}{2} \{D\}_e^T [K]_e \{D\}_e - \{D\}_e^T \{f\}_e \quad (4)$$

with $[K]_e$ and $\{f\}_e$ representing the elastic-element-stiffness matrix and the load vector, respectively. Superscript T denotes transpose of an array. From eqs (3) and (4), the element modified potential function can be expressed as

$$\psi_e = \tfrac{1}{2} \{D\}_e^T [\overline{K}]_e \{D\}_e - \{D\}_e^T \{\overline{f}\}_e + \text{constant} \quad (5)$$

where

$$[\overline{K}]_e = [K]_e + [K^*]_e$$

$$\{\overline{f}\}_e = \{f\}_e + \{f^*\}_e$$

By comparing eqs (4) and (5), one observes that the penalty-function formulation results in a simple addition of terms to the elastic-element-stiffness matrices and load vectors. The additive constant in eq (5) does not affect the minimization process. The number and symmetry of the model equations is unaltered by the inclusion of the penalty function. The global-equation assembly process is conducted in the usual way without modification.

The specific formulation used in this investigation is based on six-noded triangular elements with complete second degree polynomial displacement shape functions. This formulation ensures intra-element displacement continuity but only approaches displacement gradient continuity as the mesh is refined. Nodal averaging of gradients has been found to be effective in most cases. It is noted that, as in Refs. 2 and 15, this formulation allows one to simultaneously smooth multiple data fields.

Experimental Verification of the Smoothing Technique

The proposed methodology for optimally smoothing two-dimensional, noisy displacement data will be verified by three cases of noisy, full-field, experimental displacement data acquired using digital-image correlation. These cases are: (1) uniform rotation, (2) uniform strain, and (3) crack-tip displacement field.

In each of these cases, four different methods were used to minimize the effects of the 'unconstrained' boundary region when using the finite-element penalty method to obtain the final fit. The methods are described as follows.

(a) Full Field with no Imposed Boundary Conditions

Lines of data from the entire field of displacement data were used with the one-dimensional GCV program to estimate the optimal level of smoothing and determine the infidelity, σ_d. Then, the penalty method program was used with varying values of the smoothing parameter to fit a surface to the full field of data until the infidelity for the entire region of smoothed data equalled σ_d. No attempt was made to constrain the boundary of the smoothing region. Results from this method are shown in column 1 of Tables 1 and 2.

(b) Partial Field with no Boundary Conditions

Lines of data from the entire region were used with the one-dimensional GCV program to estimate the optimal level of smoothing and determine the infidelity, σ_d. Then, the penalty-method program was used with varying values of the smoothing parameter to fit a surface to the entire region of data until the infidelity for the central region of smoothed data (approximately 250 × 250 pixels) equalled σ_d. No attempt was made to constrain the boundary of the smoothing region by use of data. In addition, only smoothed data from the central region was used in the results, which are shown in column 2 of Tables 1 and 2.

(c) Full Field with Imposed Boundary Conditions

Lines of data from the entire field of displacement data were used to estimate the optimal level of smoothing and determine the infidelity, σ_d. In addition, displacements along the entire boundary of the region were smoothed by the one-dimensional GCV program. Then, the penalty-method program was used with varying smoothing parameters to fit a surface to the entire field of data until the infidelity for the entire region of data equalled σ_d. The analyses of the u and v displacement data by the penalty-method program was performed with the boundary constrained to have the displacements equal to the smoothed displacements. Results from this method are shown in column 3 of Tables 1 and 2.

(d) Partial Field with Boundary Conditions

Lines of data from the entire region were used to estimate the optimal level of smoothing and determine the noise level, σ_d. In addition, displacements along the entire boundary of the region were smoothed by the one-dimensional GCV program. Then, the penalty-method program was used with varying values of the smoothing parameter to fit a surface to the entire region of data until the infidelity for the central region of smoothed data (approximately 250 × 250 pixels) equalled σ_d. Analysis of both the u and v displacement data was performed with the boundary constrained to have the displacements equal to the smoothed displacements. In addition, only smoothed data from the central region were used in the results, which are shown in column 4 of Tables 1 and 2.

It is noted that the reason only interior data were chosen for (b) and (d) is that, in general, when data are smoothed the boundary data are fitted less accurately than the interior data. This makes logical sense because there are no neighboring points beyond the boundary for improved accuracy in the smooth fit to the displacement field in the boundary region. Hence, if the boundary region is excluded in the infidelity analysis and substantial differences occur between the results obtained using procedures (a) and (b) or (c) and (d), then smoothed data in the boundary region will have to be excluded. To determine whether this 'boundary' effect is present and important, sections (b) and (d) are included.

Also, the infidelity analysis was enforced over the middle 400-pixel by 400-pixel region, with the original image being 492 pixels by 512 pixels. This region was

chosen to eliminate potential problems when recording the images. For example, by choosing a region near the optical axis of the camera, curvature of the image field is minimized. Other problems that could arise during digitization of the images, such as (a) zeroes in some of the digitized lines near the edge of images and (b) movement of a portion of the image that is near the edge of the sensor plane completely out of field of view is eliminated by choosing a region near the center of the image.

It is noted that the regions near discontinuities in the displacement field (e.g., the crack line) are also excluded from the infidelity analysis. This region is excluded since one cannot acquire data by the correlation method right on the crack line; any $N \times N$ subset must reside on one side of the crack. Hence, the closest the center of a square subset can get to the crack line is $N/2$ pixels and data within the region $\pm N/2$ pixels on either side of the crack line are generally excluded. Other than the exclusion of such regions, the infidelity analysis includes all of the remaining displacement data.

Uniform Rotation Experiment

For the rotation experiment, a planar surface was rotated in-plane through increments of 0.9, 4.5 and 9.0 deg. Displacements were measured at 930 points. The data locations and the finite-element mesh for smoothing the data are shown in Fig. 1. Using the procedure outlined above, the field of displacements was smoothed. The tabulated results are presented in Table 1. The four columns in Table 1 give the results obtained from all four different methods described above.

TABLE 1—ROTATION DATA USING DIFFERENT METHODS TO MINIMIZE EFFECTS OF BOUNDARIES ON SMOOTHING RESULTS

Rotation Results (in Degrees) for Rotation Experiment Using 50 × 50 Subsets				
Rotation Measurement	Full Field with no BC's	Partial Field with no BC's	Full Field with BC's	Partial Field with BC's
0.9 ± 0.09*	0.96 ± 0.009*	0.96 ± 0.009*	0.96 ± 0.006*	0.96 ± 0.006*
4.5 ± 0.09	4.54 ± 0.015	4.54 ± 0.009	4.54 ± 0.013	4.54 ± 0.009
9.0 ± 0.09	8.99 ± 0.037	8.99 ± 0.012	8.99 ± 0.021	8.99 ± 0.008

Denotes one standard deviation

TABLE 2—COMPARISON OF STRAINS ϵ_{xx}, ϵ_{yy} AND ϵ_{xy} MEASURED BY STRAIN GAGE TO STRAINS MEASURED BY DIGITAL CORRELATION WITH PENALTY-METHOD SMOOTHING

ϵ_{xx} Results (in Microstrain) for Uniform Strain Experiment Using 50 × 50 Subsets				
Strain-gage Measurement	Full Field with no BC's	Partial Field with no BC's	Full Field with BC's	Partial Field with BC's
249 ± 1*	206 ± 120*	262 ± 129*	268 ± 160*	243 ± 128*
744 ± 2	633 ± 220	735 ± 168	742 ± 173	719 ± 162
794 ± 2	672 ± 215	737 ± 144	796 ± 169	751 ± 144
ϵ_{yy} Results (in Microstrain) for Uniform Strain Experiment Using 50 × 50 Subsets				
Strain-gage Measurement	Full Field with no BC's	Partial Field with no BC's	Full Field with BC's	Partial Field with BC's
−77 ± 1	−124 ± 113	−151 ± 131	−129 ± 124	−133 ± 121
−230 ± 1	−233 ± 134	−211 ± 129	−241 ± 136	−223 ± 132
−245 ± 1	−279 ± 165	−255 ± 193	−288 ± 194	−256 ± 187
ϵ_{xy} Results (in Microstrain) for Uniform Strain Experiment Using 50 × 50 Subsets				
Strain-gage Measurement	Full Field with no BC's	Partial Field with no BC's	Full Field with BC's	Partial Field with BC's
15 ± 1	13 ± 37	3 ± 34	−6 ± 69	1 ± 43
45 ± 1	12 ± 51	10 ± 62	7 ± 57	9 ± 56
47 ± 1	5 ± 56	3 ± 68	−5 ± 100	−5 ± 65

Denotes one standard deviation

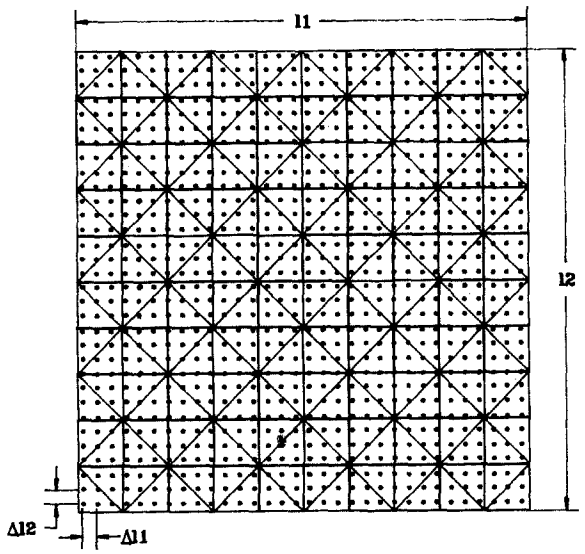

	Rotation test	Strain test
l1 (mm)	35.8	3.8
l2 (mm)	42.5	4.5
Δl1 (mm)	.90	.10
Δl2 (mm)	1.06	.12

Fig. 1—Finite-element grid and approximate input locations for smoothing analysis of rotation and uniform strain displacement data

It is noted that the full-field trends for all three data sets were found to be the same, with the edges of the 400 × 400-pixel region smoothed having nearly the same trends for all four smoothing methods. Since methods (c) and (d) require presmoothing of data on the boundary, yet does not give improved accuracy, it appears that method (b) has an advantage.

Uniform-strain Experiment

For the uniform-strain experiment, experimental-displacement data were obtained from the surface of an axially loaded aluminum specimen using digital-image correlation. The specimen's geometry is 30.5 mm × 4.04 mm × .20 mm. Digital images were obtained for axial loads of 222.5 N (50 lb), 667.5 N (150 lb) and 712 N (160 lb). The strain induced by the loading was measured using strain gages. For each of the three loadings, displacements were measured at 961 locations (31 × 31 grid using 50 × 50-pixel subsets for correlation, each subset separated by 10 pixels from its neighbor over a 300 × 300-pixel area). The data locations within the finite-element mesh for the uniform strain test are also shown in Fig. 1. Using the procedure outlined above, the field of displacements was smoothed. A comparison of the strains ϵ_{xx}, ϵ_{xy} and ϵ_{yy} measured by a strain-gage rosette to the strains obtained from the displacement fields acquired by digital correlation is shown in Table 2. The individual strain values obtained by smoothing of the displacement data were averaged over the data field to obtain the data presented in Table 2. The strains ϵ_{xx} and ϵ_{yy}, tabulated in the fourth column, are generally within five percent of the gage values. The standard deviation in the strain calculations, however, is approximately 150 μstrain at all load levels. This reflects the noise level at each point in the smoothed displacement gradients.

As with the rotation data, the full-field data for the strains obtained by each of the smoothing methods were studied. It was found that all four methods had difficulties near the edges of the 400 × 400-pixel region. However, as with the rotation data, methods (c) and (d) did not significantly improve the data near the boundary. However method (b), which excludes data near the edges of the smoothed fit from the standard deviation calculation, did improve the overall fit relative to method (a), which includes smoothed data near the boundary in the standard deviation calculation. Hence, it appears that method (b) would be the most efficient choice. It is also noted that the *average* strains obtained by method (b) are generally more accurate than the point-to-point methods, with a standard deviation of approximately 30 μstrain.

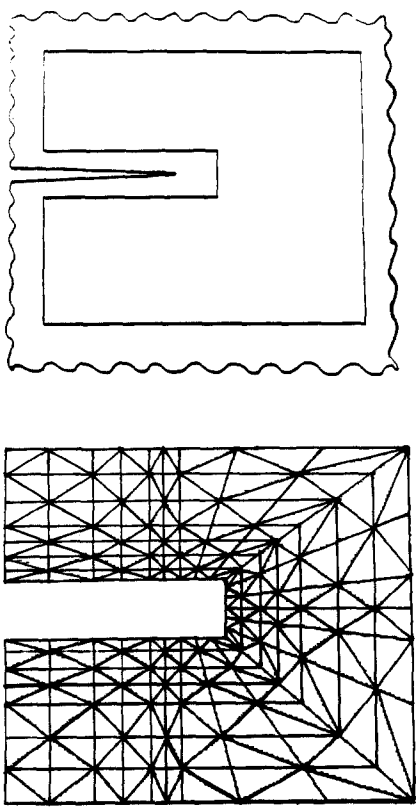

Fig. 2—Shape of region around crack tip and the finite-element grid used in smoothing of crack-tip displacement data

Crack-tip Displacement Data

Theoretical Data With and Without Noise

As a final example, the theoretical, plane strain, K_I displacement field around a crack tip was contaminated with synthetic noise and the data smoothed using the proposed technique. A schematic of both the crack-tip region to be analyzed and a typical finite-element grid used for smoothing of the data with the penalty method are shown in Fig. 2. It is noted that the grid did not span the crack flanks, thereby eliminating the displacement discontinuity. Furthermore, the grid can be used with any size data field by changing the dimensions of the boundaries.

To generate the theoretical crack-tip displacement field, a K_I value of 810 Kpa-m$^{1/2}$ was used since this value for K_I corresponded to the value for experimental data recently obtained by the authors. For the experiments, two sets of magnification factors were used. The first set, designated 3X, was 126 pixels/mm in the x direction and 150 pixels/mm in the y direction. The second set, designated 6X, was 225 pixels/mm in the x direction and 265 pixels/mm in the y direction. The region imaged was 480 pixels in the x direction and 512 pixels in the y direction and was centered around the crack tip. For the 3X case, the grid we used in the theoretical portion of this work was approximately 4.06 mm × 3.2 mm in size, with horizontal inner grid boundaries located approximately 280 μm from the crack flanks and a vertical inner-grid boundary located roughly 330 μm from the crack tip. The finite-element grid and data locations are shown in Fig. 3.

In order to verify the grid's ability to handle the K_I displacement field, a noiseless plane-strain displacement field was discretized and analyzed by the penalty-method program. The input data locations and finite-element grid used in the analysis are the same as the 3X grid shown in Fig. 3. One should note that the crack is not centered in the grid. The offset crack location was chosen for the theoretical data, since in the experiment the initial position of the crack in the experiment is offset towards the top; as the bottom edge of the specimen was displaced downwards (top edge was essentially fixed), the crack moved towards the middle of the screen. The fitted displacement solutions were almost identically the same as the theoretical displacement fields, indicating that the grid is adequate for smoothing of the displacement fields.

To determine if the smoothing procedure is adequate for estimating gradients in a complex strain field, a comparison of the theoretical $\partial v/\partial y$ gradient field to the

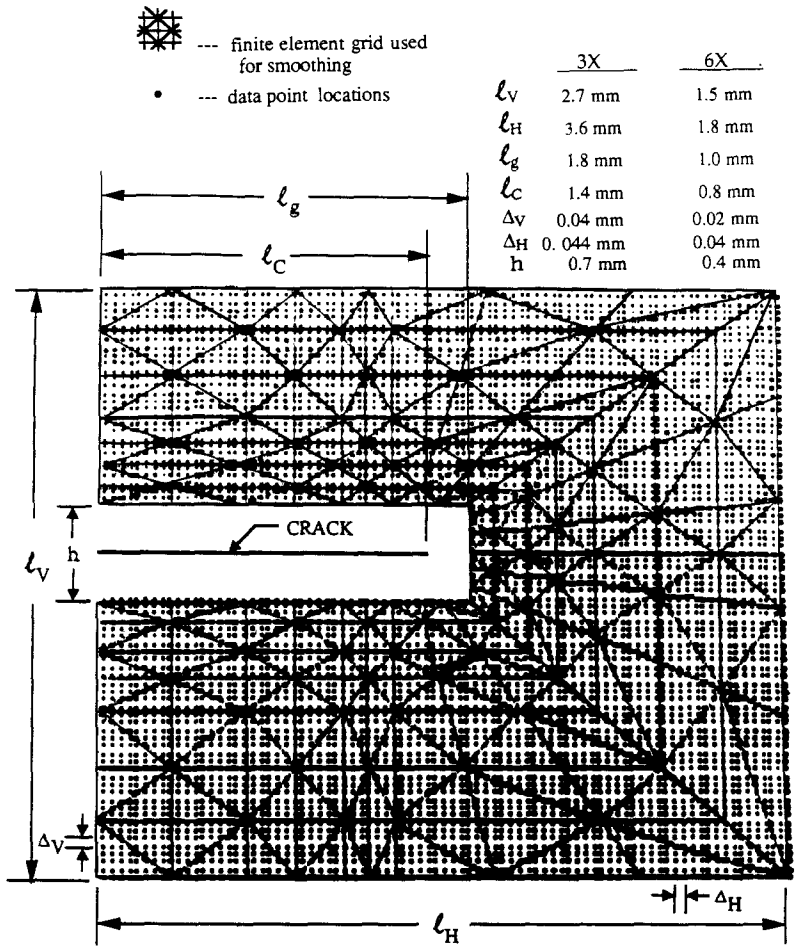

Fig. 3—Data locations inside and around finite-element grid where measured displacement data were used for smoothing analysis

Δ_V, Δ_H = spacing of points where data was acquired.

smoothed $\partial v/\partial y$ contours using method (b) is presented in Fig. 4. As expected, the gradient solution deviates at a few points near the boundaries of the grid. The solution is somewhat erratic at positions in the interior due to the fact that the gradient is constant within each element. Finally, it is noted that the rectangular cutout in the bottom figure in Fig. 4 is due to the shape of the finite-element area used for smoothing (Fig. 3); the cutout is needed since experimental data cannot be obtained for regions close to the crack line. The top figure in Fig. 4 uses a theoretical solution which is valid for the entire region and hence does not have a rectangular cutout.

It was of interest for fracture-mechanics applications to evaluate the accuracy of the J integral when calculated using the smoothed gradients. The J integral can be evaluated using the equation

$$J = \frac{G}{2}\int_\Gamma \left[\left\{R_1\left(\frac{\partial v}{\partial y} - \frac{\partial u}{\partial x}\right)\left(\frac{\partial u}{\partial x} + \frac{\partial v}{\partial y}\right) + \left(\frac{\partial u}{\partial y} + \frac{\partial v}{\partial x}\right)\left(\frac{\partial u}{\partial y} - \frac{\partial v}{\partial x}\right)\right\} dy - 2\left(\frac{\partial u \partial u}{\partial x \partial y} + R_2\frac{\partial u \partial v}{\partial x \partial x} + R_1\frac{\partial v \partial v}{\partial x \partial y}\right) dx\right] \quad (6)$$

where G is the shear modulus and R_1 and R_2 are constants characterizing the type of two-dimensional problem. For plane strain, $R_1 = 2(1-\nu)/(1-2\nu)$ and $R_2 = 1/(1-2\nu)$. For plane stress, $R_1 = 2/(1-\nu)$ and $R_2 = (1+\nu)/(1-\nu)$.

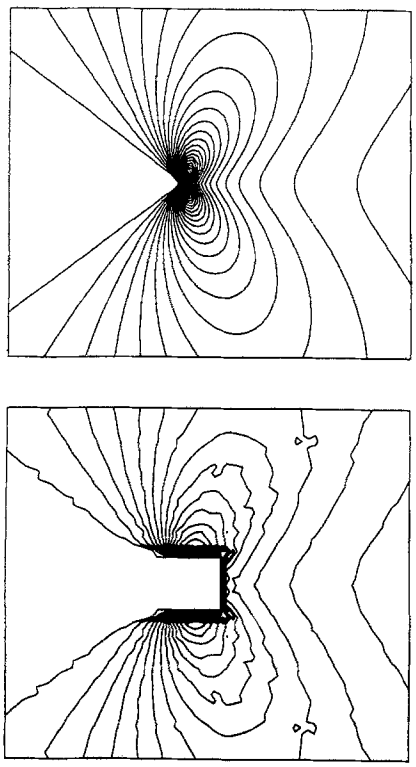

Fig. 4—$\partial V/\partial y$ contours for theoretical plane stress $\partial V/\partial y$ field and for smoothed plane stress $\partial V/\partial y$ field obtained by smoothing theoretical displacement fields. (K_I = 809.8 KPa$\sqrt{m}$ and $\partial V/\partial y$ = 1000 microstrain)

A good integration approximation can be obtained by using a finite summation and a linear interpolation of the discrete values of the terms calculated in Ref. 6. J integrals were calculated using rectangular or square contours, as shown in Fig. 5, extending from one crack flank to the other. A comparison of the theoretical J-integral values obtained using the formula $J = (K_I)^2(1-\nu)/E$ to the numerically computed values indicated that the error was less than 0.10 percent for all contours. It is noted that the J-integral values were obtained using gradient data from both the inner and outer regions shown in Fig. 5.

Next, the J integral was calculated for the plane-strain case using the penalty-solution gradients. The results, shown in Fig. 6 in an expanded scale to emphasize the small differences in the J-integral values, indicate at most a two-percent deviation from the theoretical J value for the inner contours. The reason is that the inner contours are 100 pixels × 100 pixels and extend to the inner boundaries nearest the crack flanks and not the crack

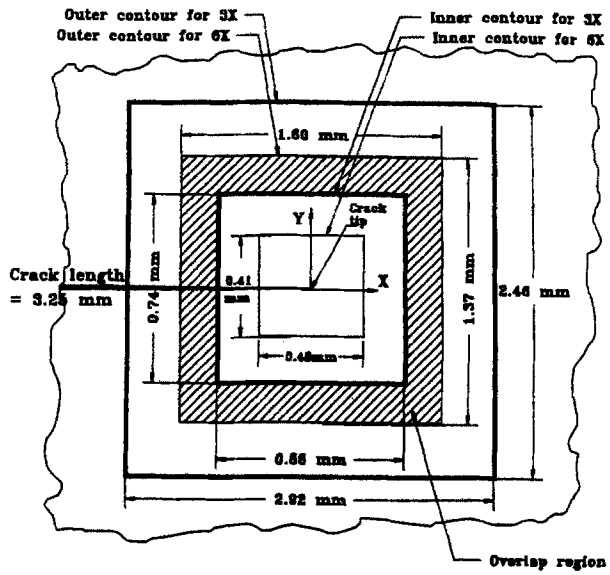

Fig. 5—Regions where displacement and displacement gradients were obtained

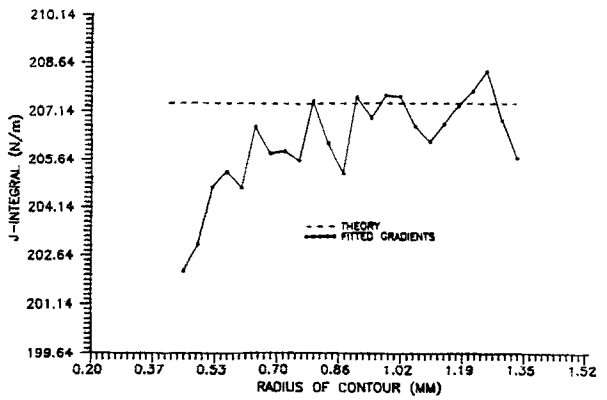

Fig. 6—Comparison of J-integral values calculated using smoothed gradients to the theoretical, plane strain J-integral value

flanks themselves. Consequently, the data which are omitted from inside the inner boundaries lie very close to the crack tip and have a much greater contribution to a smaller contour J-integral value than the crack-flank data omitted from a larger contour. This error can be reduced by omitting fewer data near the crack flanks. However, the error is small and should not degrade the noisy theoretical or experimental J-integral analyses that will be investigated. Evidently, the integration is forgiving of some noise in the gradients provided that the mean distributions are reasonable.

Experimental Crack-tip Data

After verifying the smoothing technique's ability to smooth a crack-tip displacement field using theoretical data, an experimental fracture specimen was analyzed. A Plexiglas specimen with a single edge through crack of 0.325 cm in length and located 5.08 cm from either end of the specimen is shown in Fig. 7. The specimen was subjected to uniaxial load through the pins shown in Fig. 7. Details of the experimental apparatus can be found in Refs. 13 and 14. An undeformed image was obtained at a 22.25-N preload and a deformed image was obtained at a 222.5-N loading. Magnifications of 3X and 6X are used to record images of the specimen at these loads. The region imaged for each magnification is shown in Fig. 5. The displacement field around the crack tip was then correlated using 50 × 50 subsets for both the 3X and 6X cases. The noisy u and v fields are shown in Fig. 8 for the 6X magnification. Once the displacement data are obtained, the procedure outlined above is implemented to smooth the data.

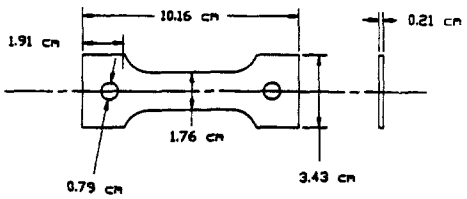

Fig. 7—Geometry of Plexiglas specimen used in J-integral experiments

For most of the displacement fields analyzed, the optimal infidelity, σ_d, was determined to be between 0.012 and 0.015 pixels. Once the optimal infidelity was determined for each displacement field, the displacement field could then be smoothed using the penalty-method program until the optimal infidelity was reached by the smoothed interior displacements.

After smoothing, the contour plots for u and v displacement for the 6X case are shown in Fig. 9. The method described above was used to smooth all crack-tip displacement data, with the boundary region eliminated from the final, smoothed fit due to inaccuracies in the gradients in this region. It is noted that presmoothing of experimental

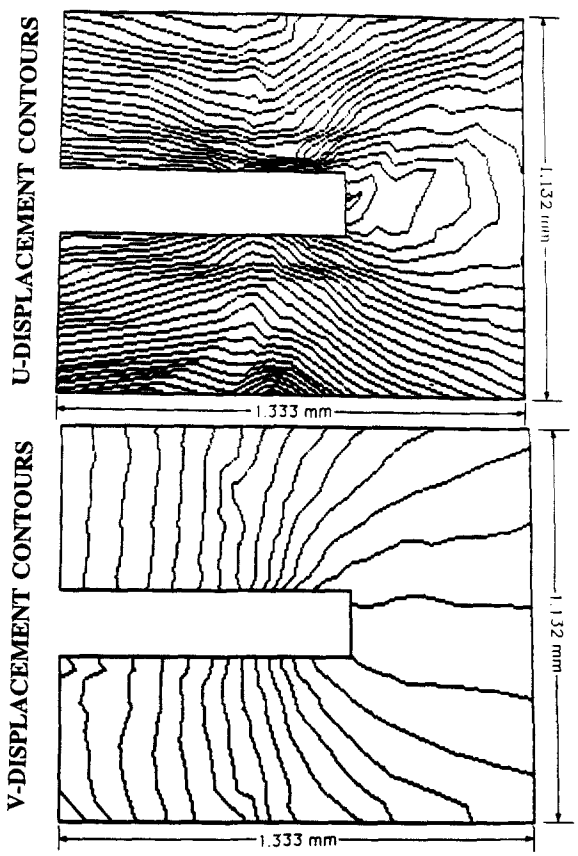

Fig. 8—Noisy experimental U and V crack-tip displacement fields for 220-N loading at 6× magnification. (U contour = 0.205 μm, V contour = 0.098 μm)

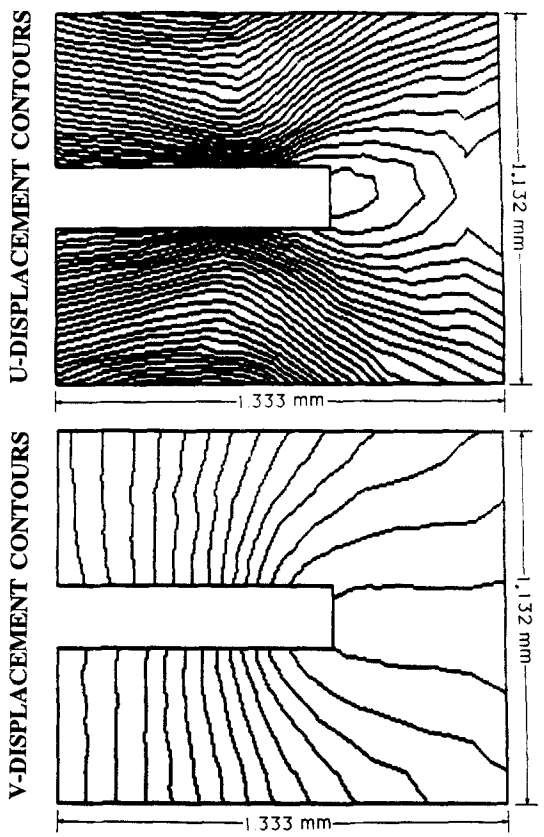

Fig. 9—Optimally smoothed experimental U and V crack-tip displacement fields for 220-N loading at 6×. (U contour = 0.171 μm, V contour = 0.991 μm)

boundary data did not improve the results in the boundary region and gave nearly identical results in the middle region. For comparison to the data, Fig. 10 presents theoretical plane-strain displacement profiles.

After two-dimensional smoothing of the displacements, the smoothed gradients were calculated in order to determine the J integral using the plane-stress version of eq (6). For loadings of 110 N, 155 N, 220 N and 265 N, J-integral contours were evaluated using rectangular contours which approximately covered the range $0.1 \leq r/t \leq 0.6$, where r is the characteristic dimensions of a contour and t is the thickness of the specimen. The J-integral results are normalized using the linear-elastic, plane-stress estimates of the J integral. The J value is computed using the formula $J_{B.C} = (K_I)^2/E$. K_I is calculated using the ASTM standard boundary collocation calculation of K_I.[16] The K_I formula is written

$$K_I = f(a'/w) \cdot \sigma\sqrt{\pi a'} \tag{7}$$

where for a finite-width specimen with a single-edge through crack,

$$f(a'/w) = 1.12 - 0.231(a'/w) + 10.55(a'/w)^2$$
$$-21.72(a'/w)^3 + 30.39(a'/w)^4$$

In these formulas, a' is the effective crack length calculated by adding the actual crack length, a, to Irwin's correction factor, Δa, where

$$\Delta a = 0.159\left(\frac{K_I}{\sigma_{ys}}\right)^2 \tag{8}$$

In addition, w is the total width of the specimen (w = 1.76 cm in Fig. 7). To normalize the radius values, the thickness of the specimen is used. In Fig. 11, the normalized J-integral results are presented. These results show almost no discernible trends as R/T ranges from 0.16 to 0.60, indicating that the J integral is not affected by three-dimensional effects. Careful inspection of Fig. 11 shows that there is a slight tendency for the curves to translate upward as the load is increased. For all loadings, the experimental J-integral values are within 20 percent of the corresponding $J_{B.C}$ values.

In addition to the J-integral values obtained for contours enclosing the crack tip, closed contours that did not enclose the crack tip were evaluated as well. According to the two-dimensional development of the J integral, the J-integral value for such closed contours should be equal to zero. Since the specimen has minimal plasticity, nonzero values probably are due to inaccuracies in the deformation gradients. Multiple contours were evaluated at locations above, below, and in front of the crack tip. The largest closed contour J-integral value was approximately 14.71 N/m, which corresponds to 6.3 percent of the $J_{B.C}$ value for the corresponding load.

Discussion of Results

By smoothing the uniform rotation and strain-displacement fields, it is apparent that the proposed smoothing technique can be used to accurately identify the noise level in experimental displacement data obtained using digital-image correlation. The noiseless displacement fields can then be reconstructed by varying the degree of smoothing until the infidelity in an interior region from

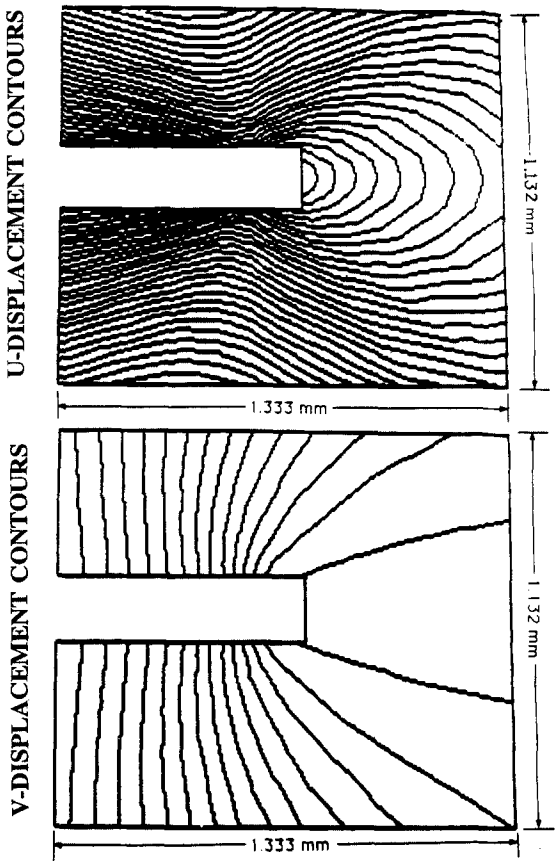

Fig. 10—U and V displacement contours for theoretical, plane strain displacement field for K_I = 810 KPa$\sqrt{m}$. (U displacement contour = 0.043 μm, V displacement contour = 0.465 μm)

the smoothed displacement fields matches the superimposed noise level. The estimated error in strain for the digital-correlation method is approximately 150 μstrain. However, displacements show large deviations from theoretical results in the boundary region up to 50 pixels away from the outer boundary. Slight improvement in the results in the boundary region is obtained by presmoothing the boundary displacements and using the resulting displacements as constraints on the penalty-method solution for the entire displacement field. This apparently reduces the size of the boundary region from 50 to 15 pixels, while altering the interior values by less than two percent. However, this procedure is inefficient due to the presmoothing. Hence, an efficient choice giving reasonable accuracy does not presmooth the data, but does emphasize the data in the center of the region for optimal smoothing.

Experimental crack-tip boundary displacements and uniform strain displacements were successfully smoothed. Analysis of both crack-tip fields and local J-integral values using the smoothed data indicate that the methodology can provide quantitative data for the assessment of near-tip deformation fields.

Conclusions

A detailed evaluation of the feasibility of determining displacement gradients from measured surface-displacement fields is completed. An improved methodology for

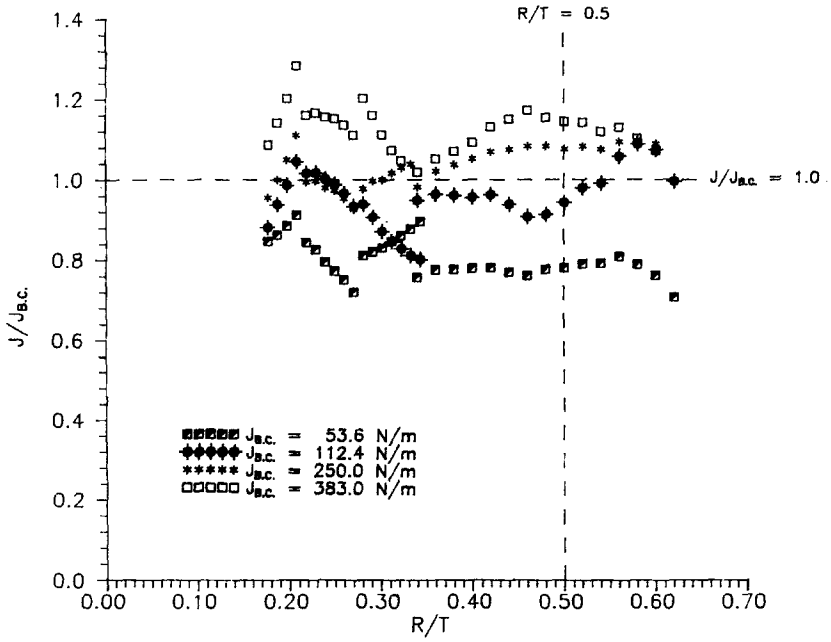

Fig. 11—$J/J_{B.C.}$ versus R/T for loadings of 110 N, 155 N, 220 N and 265 N

both the estimation and elimination of noise is proposed. The methodology is used to analyze the gradients for three tests: (1) uniform rotation, (2) uniform strain, and (3) plane strain, K_I displacement fields. Results of the study indicate that the proposed methodology can be used to reconstruct noisy two-dimensional displacement data and their corresponding gradients. Specifically, it is shown that (a) the digital-correlation method for acquiring displacement fields has a point-to-point error in strain of approximately 150 μstrain, (b) the error in the *average strain* in a region of uniform strain is on the order of 30 μstrain, (c) the displacement 'noise' present in digital correlation is very small, approximately 0.01 pixels, (d) the proposed methodology for reducing noise in the data is essential to the accurate evaluation of displacement gradients, (e) the successful evaluation of displacement and displacement gradients for all three cases indicates that the proposed methodology can be used both to quantify the displacement fields and to reasonably estimate the overall gradient trends, and (f) application of the methodology to experimental crack-tip data in the region $0.15 \leq (r/t) \leq 0.60$ demonstrates that the two-dimensional J-integral value is not affected by three-dimensional effects.

Acknowledgments

The authors wish to thank Dr. Albert Kobayashi and Dr. Oscar Dillon, former directors of the Solid Mechanics division with the National Science Foundation, for their continual encouragement and support. Also, the financial support of the National Science Foundation through grant #ENGR-PYI-8451017 is greatly appreciated. Finally, the assistance of Mr. Guang Ma and Mr. Hang Gang has been important to the completion of the work.

References

1. Segalman, D.J., Woyak, D.B. and Rowlands, R.E., "Smooth Spline-like Finite-element Differentiation of Full-field Experimental Data over Arbitrary Geometry," EXPERIMENTAL MECHANICS, **19** *(12), 429-437 (1979).*

2. Feng, Z. and Rowlands, R.E., "Continuous Full-field Representation and Differentiation of Three-Dimensional Experimental Vector Data," Comp. and Struct., **26** *(6), 979-990 (1987).*

3. Rowlands, R.E., Winters, K.D. and Jensen, J.A., "Full-Field Numerical Differentiation," J. Strain Analysis, **13** *(3), 177-183 (1978).*

4. Tessler, A., Freese, A., Anastasi, R., Serabian, S., Oplinger, D. and Katz, A., "Least-Squares Penalty-Constraint Finite Element Method for Generating Strain Fields from Moire Fringe Patterns," Proc. 1987 SPIE Conf. on Photomechanics and Speckle Metrology, 814, 314-323 (1987).

5. Englestad, M.J., Chambless, D.A., Swinson, W.F. and Turner, J.L., "Hybrid Stress Analysis of Vibrating Plates Using Holographic Interferometry and the Finite-element Method," EXPERIMENTAL MECHANICS, **27** *(1), 23-30 (1987).*

6. Wahba, G., "Smoothing Noisy Data by Spline Functions," Numerische Mathematik, **24**, *383-393 (1975).*

7. Craven, P. and Wahba, G., "Smoothing Noisy Data with Spline Functions: Estimating the Correct Degree of Smoothing by the Method of Generalized Cross Validation," Numerische Mathematik, **31**, *377-405 (1979).*

8. Busby, H.R. and Dohrmann, C.R., "Algorithms for Smoothing Noisy Data with Spline Functions and Smoothing Parameter Selection," Proc. VI Int. Cong. on Exp. Mech., **II**, *843-849 (1988).*

9. Dohrmann, C.R. and Busby, H.R., "Spline Function Smoothing and Differentiation of Noisy Data on a Rectangular Grid," Proc. 1990 SEM Spring Conf. on Exp. Mech., 76-84 (1990).

10. Sutton, M.A., Cheng, M., Peters, W.H., III, Chao, Y.J. and McNeill, S.R., "Application of an Optimized Digital Correlation Method to Planar Deformation Analysis," Image and Vision Computing, **4**, *143-150 (1986).*

11. Bruck, H.A., McNeill, S.R., Sutton, M.A. and Peters, W.H., III, "Digital Image Correlation Using Newton-Raphson Method of Partial Differential Corrections," EXPERIMENTAL MECHANICS, **28** *(3), 261-267 (1989).*

12. Bruck, H.A., McNeill, S.R., Russell, S.S. and Sutton, M.A., "Use of Digital Image Correlation for the Determination of Displacements and Strains," Nondestructive Testing of Aerospace Requirements, ed. G.L. Workman, Gordon and Breach, 99-111 (1989).

13. Sutton, M.A., Turner, J.L., Chae, T.A. and Bruck, H.L., "Development of a Computer Vision Methodology for the Analysis of Surface Deformations in Magnified Images," ASTM STP 1094: MICON 90, Advances in Video Technology for Microstructural Control (1990).

14. Sutton, M.A., Turner, J.L., Chae, T.A. and Bruck, H.L., "Experimental Investigations of Three-Dimensional Effects Near a Crack Tip Using Computer Vision," Int. J. Fract. (1990).

15. Chambless, D.A., Suhling, J.C., Swinson, W.F. and Turner, J.L., "A New Hybrid Photoelastic-Finite Element Technique for Stress Analysis," Proc. 1986 SEM Spring Conf. on Exp. Mech., 991-999 (1986).

16. Paris, P.C. and Sih, G.C., "Stress Analysis of Cracks," ASTM STP 391, 30-81 (1965).